Wiley
Journal of Nanotechnology
Volume 2024, Article ID 6623255, 10 pages
https://doi.org/10.1155/2024/6623255

WILEY

Research Article

Low Temperature Synthesis of Hexagonal Bi_2Te_3 Nanoplates Using an Open Reactor and Its Effect on Their Physicochemical Properties

Laura A. Reyes-Verdugo,[1] Maria de J. Martinez-Carreon,[1] C. D. Gutierrez-Lazos,[1] Francisco J. Solis-Pomar,[1] Jose G. Quiñones-Galvan,[2] and Eduardo Perez-Tijerina[1]

[1]*Centro de Investigacion en Ciencias Fisico Matematicas, Facultad de Ciencias Fisico Matematicas, Universidad Autonoma de Nuevo Leon, Av. Universidad s/n. Ciudad Universitaria 66455, San Nicolas de los Garza, Nuevo Leon, Mexico*
[2]*Departamento de Fisica, Centro Universitario de Ciencias Exactas e Ingenierias, Universidad de Guadalajara, Boulevard Marcelino Garcia Barragan 1421, Guadalajara 44430, Mexico*

Correspondence should be addressed to C. D. Gutierrez-Lazos; claudio.gutierrezl@uanl.edu.mx

Received 26 January 2024; Revised 19 July 2024; Accepted 5 August 2024

Academic Editor: Marco Rossi

This report presents the physicochemical properties of hexagonal Bi_2Te_3 nanoplates chemically prepared in an open reactor at a lower temperature (140°C) than those reported for controlled condition techniques. The samples were drop-cast on glass and FTO substrates for subsequent structural, chemical, and thermoelectric analyses. The electron microscopy analysis demonstrated that samples precipitated in highly crystalline hexagonal nanoplates, grown along the [0 1 5] plane of the rhombohedral phase of Bi_2Te_3. The nanoplates exhibited an extension of up to several hundred nanometers, with thicknesses in the range of 20–40 nm, and with an interplanar spacing of 0.321 nm. A vibrational mode at 120 cm^{-1} due to the breaking of the symmetry of the Bi_2Te_3 crystal along the C axis was observed by Raman spectroscopy. XPS results showed that despite the strong reactivity of Te^{2-} ions with ambient oxygen, the crystallization of Bi_2Te_3 hexagonal nanoplates is feasible without controlled vapor pressure and at a lower temperature than reported in other works. Finally, the measurement of the Seebeck coefficient exhibited a *p*-type conductivity of Bi_2Te_3, with a maximum value of 169 μV/K within the temperature range of 300 to 320 K.

1. Introduction

The increasing demand for small-scale and portable energy generation systems has become a priority. While it is well established that various heat-generating processes, such as those associated with transportation, industry, domestic activities, and even the human body, produce substantial waste energy, the pursuit of a sustainable approach to utilize this residual heat is of utmost importance [1, 2].

The use of heat recovery has been widely adopted since the invention of thermal machines. However, emerging technologies necessitate affordable and modular systems for converting heat into electricity. Thermoelectric (TE) devices have garnered significant attention as an alternative power source, as they can be readily manufactured. The conversion of heat to electricity in thermoelectric materials is attributed to their solid-state energy conversion device design, which features n-type and p-type semiconductor heterostructures, enabling the transformation of heat into electrical power. This property can therefore be exploited for the recovery of waste heat. The fundamental principle underlying thermoelectric power generation is the Seebeck effect: when a material is subjected to a temperature gradient, it experiences the generation of an electric potential, resulting in the detection of an electrical current. Consequently, a high Seebeck coefficient is desirable [3–5].

The efficiency of a TE device is related with a unique material-dependent dimensionless property known as the figure of merit $ZT = S^2\sigma T/k$, where T is the absolute temperature, σ the electrical conductivity, S the Seebeck coefficient, and κ the thermal conductivity. The portion of the numerator, $S^2\sigma$, is referred to as the power factor [6, 7]. To maintain a large temperature gradient across the material and facilitate electrical carrier transport through it, low thermal conductivity k and high electrical conductivity σ are desirable intrinsic thermoelectric material properties. Different semiconductor materials have been studied over the past decades, demonstrating the advantages of nanostructured materials due to their superior mechanical properties compared to single crystals which are more fragile [6], maximizing the TE figure of merit, with a high σ and S and low κ [8–10].

There are several methods or techniques to synthesize thermoelectric nanomaterials; i.e., pulsed laser processing [11], flash evaporation [12], and physical vapor deposition methods, such as sputtering [13, 14] are common methods to fabricate TE films. Based bottom-up techniques seem to be a good alternative since they are low-cost and commercially scalable, including wet chemistry methods such as solvothermal [15, 16], and microwave-assisted [17–20]. Bismuth telluride (Bi_2Te_3) and related alloys have been extensively utilized as thermoelectric materials, as they can achieve superior performance near room temperature [16]. In addition, Bi_2Te_3 can be employed as a topological insulator when fabricated as ultrathin nanoplates, owing to its unique surface state electronic properties [21–23].

Bi_2Te_3 is a material of the tetradymite family. It has a rhombohedral crystal structure belonging to space group D^5_{3d} ($R\bar{3}m$) [24]. The Bi_2Te_3 unit cell is a hexagonal structure, where each charge-neutralized layer consists of five covalently bonded monatomic sheets aligned in the C direction, according to the sequence $Te^{(1)}$—Bi—$Te^{(2)}$—Bi—$Te^{(1)}$, defined as the *quintuple layers* [25]. This characteristic is due to the high c-axis to a-axis length ratio in the crystal structure [26, 27], which allows the growth of hexagonal Bi_2Te_3 nanostructures with high crystallinity along the basal plane. This encourages a low thickness of the hexagonal structure, which enhances the electrical conductivity through the reduction of thermal conductivity by the scattering of phonons [16].

It has been proven for Bi_2Te_3 nanocrystals synthesis, that using wet chemical techniques results in a higher power factor, i.e. the microwave-assisted technique, and the solvothermal method [17, 28, 29]. According to Wang et al. [30], this improvement in the power factor does not apply to thin films, highlighting the need for the optimization of deposition techniques for Bi_2Te_3 nanostructured thin films.

In this research, we successfully synthesized Bi_2Te_3 nanoplates using a simple and cost-effective method, without the need for expensive equipment such as vapor pressure control systems or microwave irradiation, this approach allowed us to produce the bismuth telluride nanoplates at a significantly lower temperature compared to previous studies [15–20]. Although other researchers such as Sun et al. [31] and Srivastava and Singh [32] have reported low-temperature synthesis of Bi_2Te_3, they did not obtain the hexagonal nanoplate structure. In contrast, the present work demonstrates the feasibility of producing Bi_2Te_3 hexagonal nanoplates through a relatively simple method involving low-temperature heat treatment in a convection oven under atmospheric pressure. Synthesis conditions such as concentration of capping agent [3], heating time, temperature, and the cleaning process were evaluated. Morphology and crystallographic structure of nanoplates were also analyzed.

2. Experimental

2.1. Chemicals. The reagents used were bismuth nitrate pentahydrate ($Bi(NO_3)_3{\cdot}5H_2O$, >99.9%), sodium tellurite (Na_2TeO_3, >99.5%), sodium hydroxide (NaOH, >99%), poly (vinyl pyrrolidone) (PVP, MW ≈40 000), and ethylene glycol (EG). All reagents were purchased from Sigma-Aldrich and were used as received, without further purification.

2.2. Preparation of Crude Solution. Bismuth telluride was synthesized following a modified solvothermal process [33, 34] by mixing solutions in 10 mL EG of 0.2 mmol Bi $(NO_3)_3{\cdot}5H_2O$, 0.3 mmol Na_2TeO_3, and 4 mmol sodium hydroxide (NaOH). PVP was used as a capping agent in different concentrations, labeled as PVP_n ($PVP_1 = 2.78\,\mu$mol, $PVP_2 = 5.55\,\mu$mol, and $PVP_3 = 11.1\,\mu$mol). Compared to the reagents used in prior studies, we utilized more cost-effective and readily available bismuth nitrate pentahydrate as the bismuth precursor, rather than the bismuth chloride employed by He and collaborators [33]. In addition, we used ethylene glycol as the solvent, in contrast to the water and alcohol mixtures utilized by Zhang et al. [34]. Three main solutions, referred to as D1, D2, and D3 were prepared by dissolving Bi $(NO_3)_3{\cdot}5H_2O$ (D1), Na_2TeO_3 (D2), and NaOH (D3), in 10 mL EG, ultrasonically stirred until transparent solutions were obtained. Then, PVP_n was added to the D1 solution, with magnetic stirring required until it was completely dissolved; this new solution is referred to as D4. The D2 solution was then added to D4, forming a milky solution known as D5. Finally, the crude solution (D6) was prepared by mixing D3 and D5 until a completely transparent and homogenous solution was obtained (Figure 1). The mixture was placed in a simple convection oven at 140°C for 48 h with no vapor pressure control. The resulting products exhibited a dark gray tonality. The mixture was then centrifuged at 10 000 rpm for 10 min after the addition of DI water. The supernatant was removed, and the solid phase was dispersed in isopropanol assisted by sonication. The washing steps were repeated with ethanol to remove the excess ethylene glycol, PVP, and other impurities. The final product was dispersed in isopropanol for further characterization.

2.3. Drop Casting Deposition of Bi2Te3 Film. Aliquots of Bi_2Te_3 dispersion in isopropanol were dropped on a 1 cm^2 surface area of a BK7 glass substrate to achieve deposition. These samples were analyzed by SEM, Raman spectroscopy, XRD and XPS. In addition, another deposition of Bi_2Te_3 was

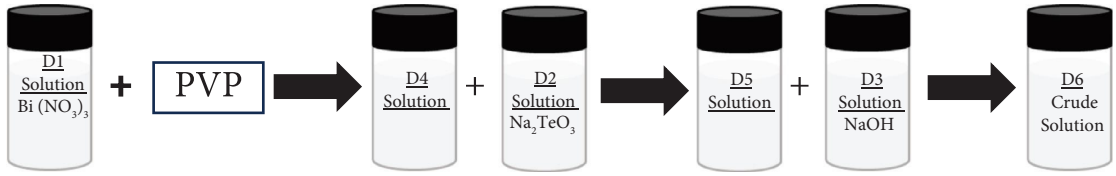

Figure 1: Preparation of crude solution to obtain Bi_2Te_3 hexagonal nanoplates.

carried out on fluorine-doped tin oxide (FTO)- coated glass slide (~7 Ω/sq, Sigma-Aldrich) for the Seebeck coefficient measurement.

2.4. SEM/TEM Analysis. The microstructure of Bi_2Te_3 nanoplates was analyzed with a field emission scanning electron microscope (FESEM) FEI NOVA nanoSEM200, with a HV of 10.00 kV and magnifications of 20,000 and 30,000x. The precise structure of the nanoplates was analyzed with a high-resolution transmission electron microscope (HRTEM) JEOL JEM2100, with an accelerating voltage of 200 kV.

2.5. Raman Analysis. Raman light scattering measurements were performed using a Thermo Scientific DRX2 Smart Raman spectrometer equipped with a 785 nm laser and a maximum output power of 250 mW.

2.6. X-Ray Diffraction. An X-ray diffraction (XRD) pattern for Bi_2Te_3 depositions on BK7 substrates was obtained on a Panalytical X'Pert^3 Powder X-ray diffractometer with Cu K_α radiation ($\lambda = 1.5405$ Å).

2.7. FTIR Analysis. The Fourier transform infrared (FTIR) spectra were obtained using Thermo Scientific Nicolet IS50 FTIR. The sample was scanned in the wavenumber range of 400–4000 cm^{-1}.

2.8. XPS Analysis. X-ray photoelectron spectroscopy (XPS) analysis was performed using a Phoibos 150 (Specs) analyzer with a monochromatic Al K_α source (1486.69 eV) at 250 W and 12.5 kV. The instrument utilized a 1D DLD detector and a flood gun operating at 20 mA and 2 eV.

2.9. Thermoelectric Characterization. The Seebeck coefficient of the Bi_2Te_3 deposition was directly measured across the temperature range of 302 K to 423 K using a homemade system described by Díaz-Torres et al. [35], utilizing two chromel/alumel thermocouples as both contact points and to register the temperature and thermo-voltage.

3. Results and Discussion

3.1. SEM/TEM Analysis. Scanning electron microscopy (SEM) and transmission electron microscopy (TEM) were employed to investigate the size, morphology, and crystal structure of Bi_2Te_3 nanoplates synthesized at 140°C. Figures 2(a) and 2(b) present SEM images of the nanoplates, revealing their hexagonal shape with an extension of up to several hundred nanometers, and thickness minor than the Bohr radius of the Bi_2Te_3 exciton (57 nm) [36]. Figure 2(d) displays an HRTEM image taken from the top left section of the nanoplate exhibited in Figure 2(c). The analysis of this micrograph (Figure 2(d)) shows structurally uniform lattice fringes. The crystallographic distance profile obtained for this section of nanoplate (Figure 2(e)) indicated an interplanar spacing of 0.321 nm, corresponding to the [0 1 5] plane of the rhombohedral structure of Bi_2Te_3 (JCPDS File NO. 00-015–0863 from ASTM), indicating that this nanoplate has a preferential orientation along with [0 1 5] direction belonging to the trigonal R$\bar{3}$m structure of Bi_2Te_3 [16, 34, 37].

3.2. Raman Analysis. It has been widely reported that the unit cell of Bi_2Te_3, belonging to the trigonal R$\bar{3}$m structure, has a primitive cell with five atoms [24, 38–40]. According to Richter [40], Bi_2Te_3 bulk crystals reveal 3 acoustic and 12 optical phonon vibrational modes. Figure 3 exhibits the Raman spectrum of synthesized Bi_2Te_3 nanoplates. The labeling of the observed peaks indicates the frequencies A^1_{1g}, E^2_g, A^2_{1g}, and A^2_{1u} (LO), which are consistent with other reports on the synthesis and study of bidimensional structures of Bi_2Te_3 [41–44], for instance, the location of the vibrational mode A^1_{1g} around 59 cm^{-1} is reported for two-dimensional Bi_2Te_3 structures [45]. The letters "E" and "A" correspond to the in-plane and out-of-plane (c-axis) lattice vibrations (i.e., perpendicular to the film plane), respectively. The subscript "g" denotes Raman-active modes, while "u" stands for IR-active modes [44, 46]. In this nomenclature, LO refers to longitudinal optical phonons which are active in the IR wavelength range and belong to the phonon zone-boundary (Z point) [40, 47]. According to Yu and Cardona [48], in crystals with inversion symmetry, the IR-active modes, such as A^2_{1u}, must be odd parity, while the Raman-active modes E^2_g, A^1_{1g} must be even parity under inversion.

On the other hand, it is reported that the ratio between the intensities of the vibrational modes A^1_{1g} and E^2_g, that is, $I(A^1_{1g})/I(E^2_g)$, increases when the Bi_2Te_3 structure is on the order of a few quintuple layers. According to the Raman spectrum of Figure 3, this ratio is equal to 0.811, which is indicative of the thickness of the nanoplates shown in Figure 2(b) [45].

It is known that the phonon displacement vector Q of an odd-parity phonon (IR) changes the sign under inversion [47]. As shown in Figure 4, modes E^2_g and A^1_{1g} are twofold degenerate: in E_g, the atoms vibrate in the basal plane. The appearance of A^2_{1u} mode in the sample is due to the breaking

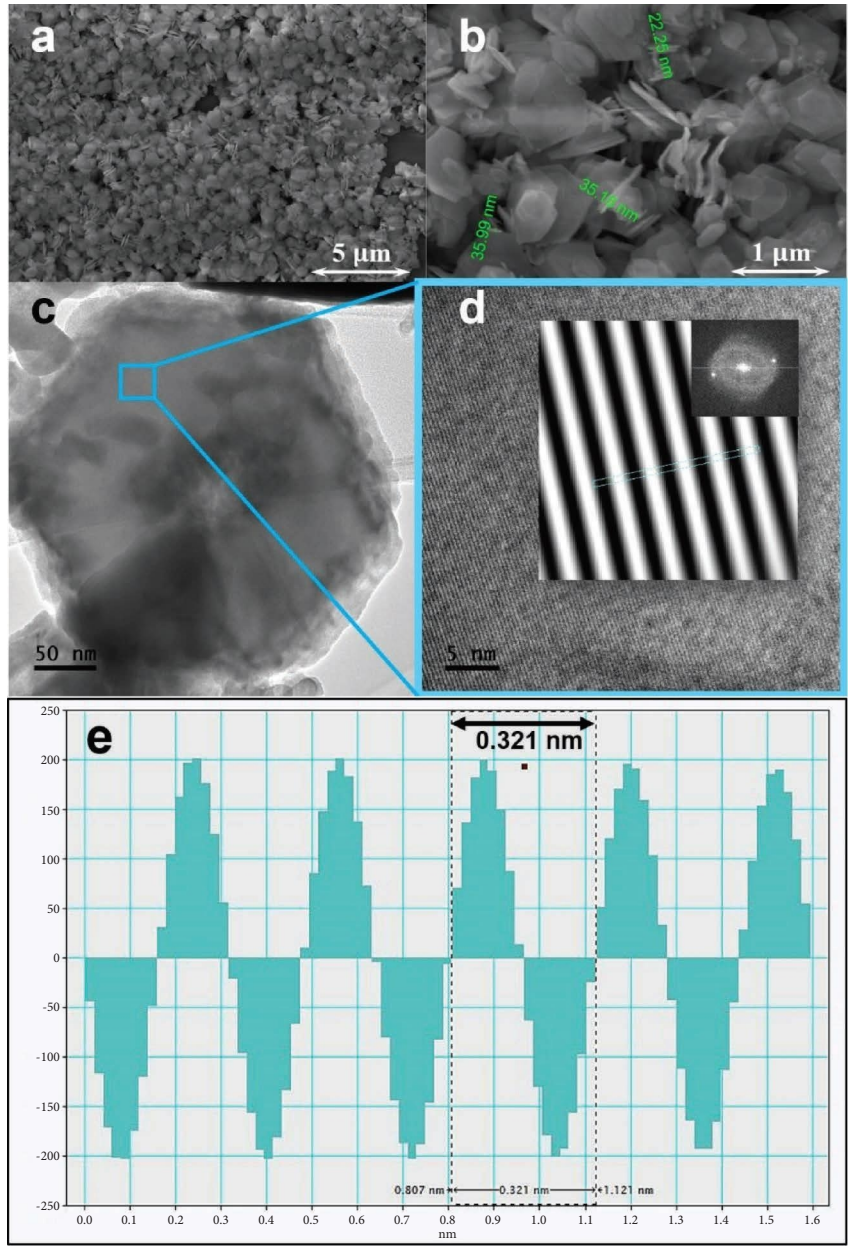

FIGURE 2: (a) SEM images of the Bi_2Te_3 nanoplates synthesized without controlled vapor pressure at 140°C, (b) SEM images of Bi_2Te_3 show the nanoplate thicknesses from ≈22 to ≈35 nm, (c) bright-field TEM micrograph of an individual Bi_2Te_3 nanoplate exhibits its hexagonal shape, and (d) the corresponding HRTEM image of a hexagonal nanoplate is shown in (c). (e) The crystallographic distance profile obtained for the section of Bi_2Te_3 nanoplate exhibited in (d).

of the crystal symmetry along the c-axis, allowing the formation of the ultra-thin thickness hexagonal nanoplates [49], as shown by the SEM micrograph of Figure 2(b).

3.3. X-Ray Diffraction. The X-ray diffraction pattern obtained for a Bi_2Te_3 deposition is shown in Figure 5. Contrary to the results obtained by Raman spectroscopy, the X-ray diffraction pattern indicated the presence of a secondary phase, specifically tellurium. No additional phases were detected. The indexing of diffraction peaks revealed the presence of the rhombohedral phase of Bi_2Te_3 ($R\bar{3}m$ group), according to the JCPDS card 00-015-0863. This structure exhibited a preferential orientation in [0 1 5] direction as reported for the synthesis of Bi_2Te_3 hexagonal nanoplates [33, 50], with the peak located at 27.57°. The secondary crystalline phase corresponded to the hexagonal $P3_121$ structure of tellurium (Te), according to the JCPDS card 00-036-1452. The unlabeled peak located at 28.22° (∗) has been reported as reflection of the [0 1 5] plane of the rhombohedral phase of Bi_2Te_3 [51].

Since our samples were prepared in a simple convection oven, under ambient conditions, and at a low temperature, the precipitation of elemental tellurium is possible. It has been

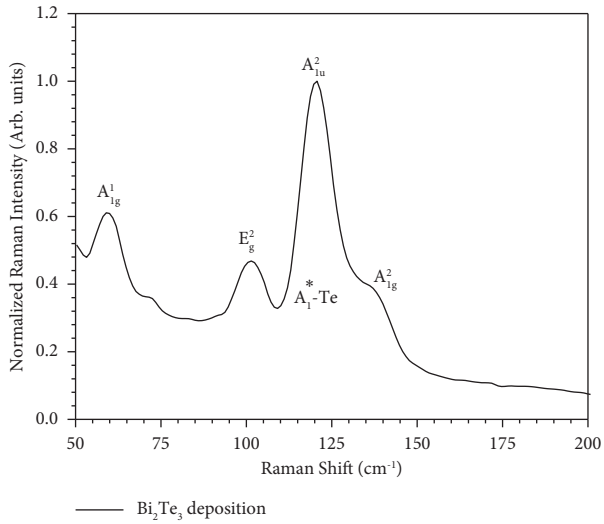

FIGURE 3: Raman spectrum of Bi_2Te_3 hexagonal nanoplates.

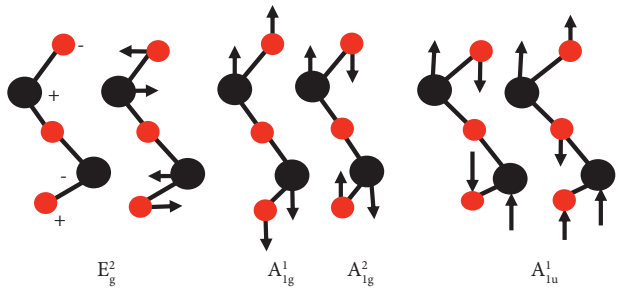

FIGURE 4: Schematic diagram of the main lattice vibrations in Te-Bi bounds of Bi_2Te_3. Black circles are Bi atoms, and red circles are Te atoms. The middle Te atom works as a center for the inversion symmetry. The signs indicate atomic motions toward and from the observer.

reported that the oxidation of the telluride chemical precursor leads to the formation of tellurium nanorods [52]. These structures have the hexagonal phase and exhibit a Raman spectrum where the main vibrational modes are labeled as A_1 an E. The A_1 mode is visible in the 119–122 cm^{-1} range as a narrow and highly intense peak [53]. However, the peak corresponding to A^2_{1u} vibrational mode of Bi_2Te_3, located at 120.7 cm^{-1}, was broadened and highly intense; therefore, the A_1 mode of tellurium was not observable. Likewise, it has been reported that the E mode is located around 139.7 cm^{-1} [53]; nevertheless, this peak was not observed.

In addition, several reports indicate that hexagonal Bi_2Te_3 nanoplates crystallize starting from tellurium nanorods, suggesting that in the initial stage of the Bi_2Te_3 synthesis, tellurium precipitates in the form of nanorods, serving as a precursor to the tellurium ion [54–56]. This process is most frequently observed in syntheses where bismuth chloride is used as a precursor of the bismuth ion. Based on the size dispersion of the nanoplates shown in the SEM micrographs in Figures 2(a) and 2(b), we can infer that synthesis at low pressure and temperature tends to slow down the crystallization process of the Bi_2Te_3 nanoplates, resulting in some tellurium remaining unused.

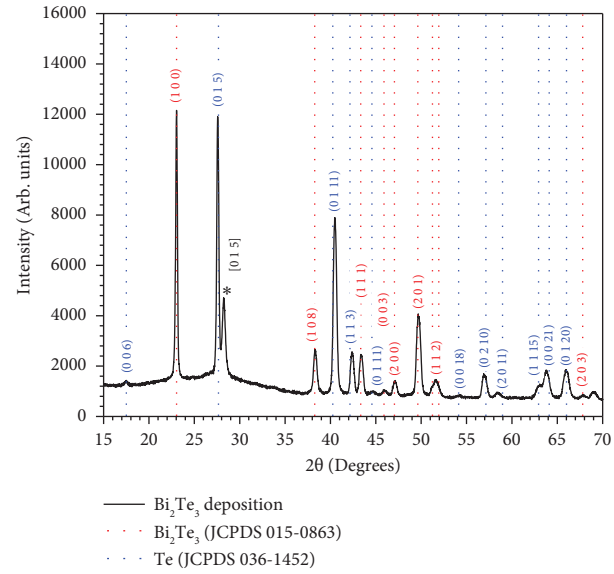

FIGURE 5: X-ray diffraction pattern of a deposition of Bi_2Te_3.

3.4. FTIR Analysis. The FTIR spectrum of a Bi_2Te_3 deposition is shown in Figure 6. In this spectrum, it is possible to appreciate a widened and strong peak at 642 cm^{-1}, which has been assigned to the Bi-O bond for samples synthesized by hydrothermal route [57, 58], consequently, the formation of these bonds may be due to environmental oxidation. The remaining observed bands correspond to the vibrational modes of the pure PVP [54], i.e., the C–H bending at 817, 880, and 950 cm^{-1}. The peaks found at 1050,–1150 cm^{-1} correspond to the C-N bond. The vibrational modes located at 1378, 1466, 2882, 2931, and 2969 cm^{-1} are assigned to the bending and stretching vibrations of C-H bounds. Finally, the strong and broad peak around 3330 cm^{-1} corresponds to the O-H bond of the EG [57, 59]. Notably, the band at 1648 cm^{-1} assigned to C=O bond of PVP is reduced. This decrease suggests a stabilization of Bi_2Te_3 hexagonal nanoplates by the PVP molecule [54].

3.5. XPS Analysis. The chemical characterization results by XPS are shown in Figure 7, where the spectra of a thin film sample fitted with Gaussian curves can be observed. The XPS survey spectrum for the binding energy range from 0 to 1300 eV is shown in Figure 7(a). The peaks shown in the survey spectrum were identified as corresponding to the elements Te, Bi, C, and O.

Figure 7(b) shows the high-resolution XPS scan of Bi_{4f} doublet peaks centered near 158.5 and 164 eV corresponding to Bi $4f_{7/2}$ and Bi $4f_{5/2}$, respectively. The peaks can be deconvoluted into two signals centered at 157.6 eV and 162.9 eV, which are associated with Bi-Te bonds, confirming the formation of the Bi_2Te_3 phase [60–62]. In addition, two peaks centered at 158.6 eV and 163.9 eV coincide with those reported for bismuth oxide (BiO_x) peaks, suggesting the possible formation of a surface oxidation layer [60, 61]. Furthermore, the Te 3d peaks are exhibited in Figure 7(c) whose curve contains two doublets that can be deconvoluted

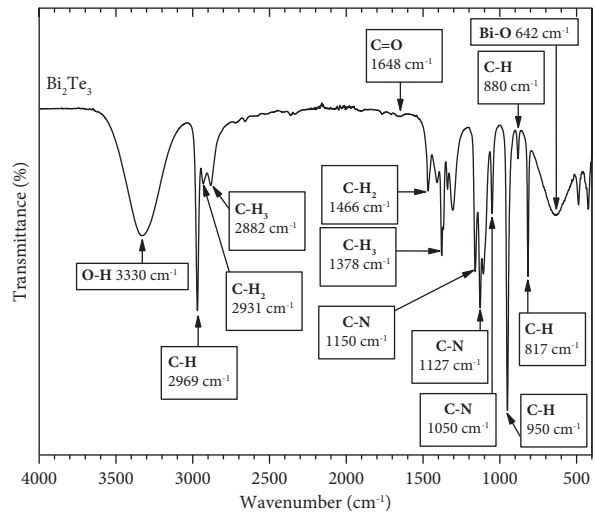

Figure 6: FTIR spectrum of Bi_2Te_3 hexagonal nanoplates.

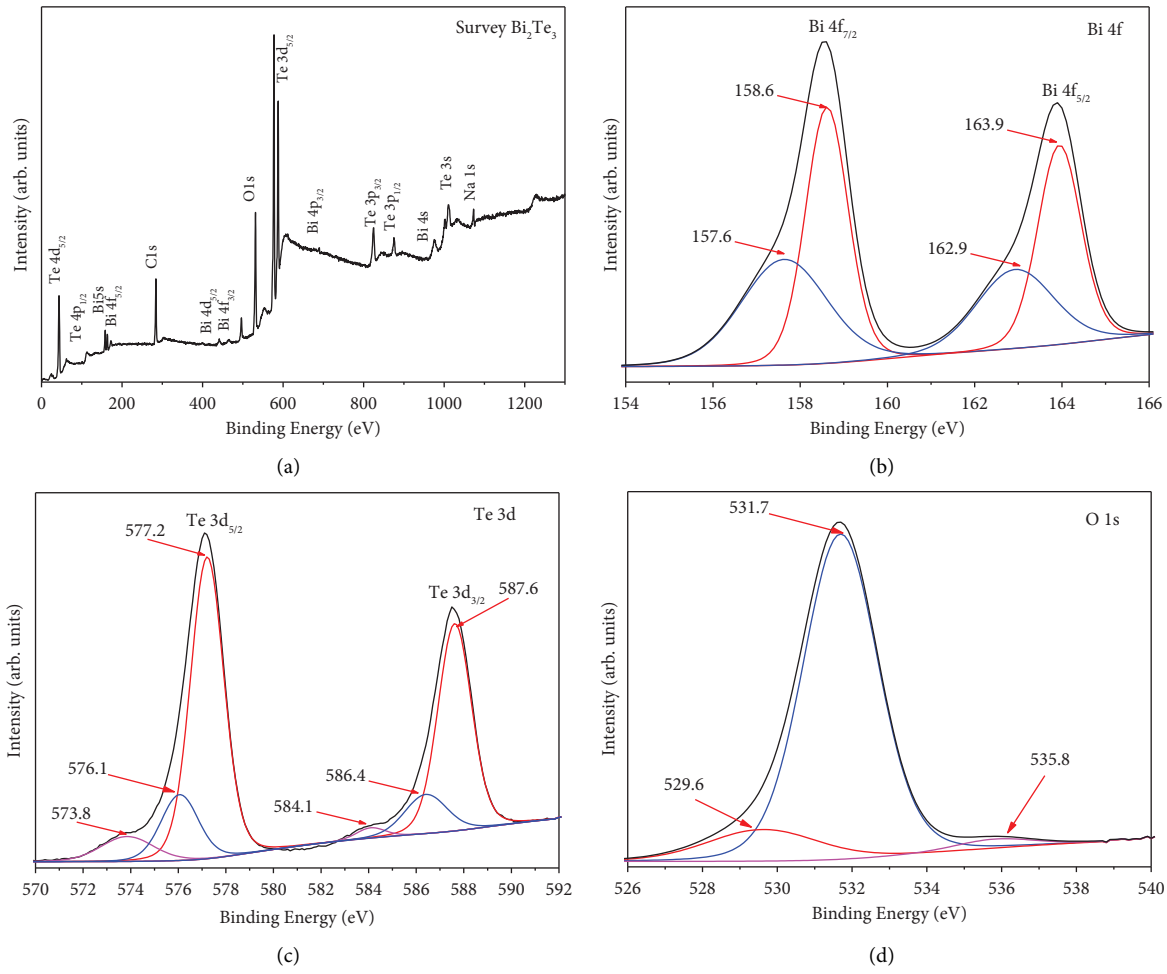

Figure 7: XPS spectra for Bi_2Te_3 hexagonal nanoplates: (a) the survey spectrum where Bi, Te, and O peaks are resolved. (b–d) High-resolution scans around the Te 3d, Bi 4f, and O 1s main peaks, respectively.

into three component peaks for each. The peaks centered at 573.8 eV and 584.1 are representative peaks of the Bi_2Te_3 phase. Likewise, we have two peaks centered at 576.1 and 586.4 eV are attributed to the Te^{4+} state, possibly due to the TeO_2 phase formation, while the peaks centered at 577.2 and 587.6 eV correspond to the Te^{+6} (TeO_3), also likely a result of surface oxidation [60–65]. The observed peak positions and relative intensities are consistent with previously reported Bi_2Te_3 samples in the literature [60–62].

Additionally, the C 1s and O 1s peaks also are observed in the XPS spectrum of the sample, where the C-C and C-O bonds (localized at 284.1 and 531.7 eV, respectively) exhibit significant intensity compared to the remaining peaks [66–68]. The C peaks likely arise from the laboratory environment, while the oxygen peaks confirmed the natural tendency of Te^{2-} precursors to react with the environmental air, inducing surface oxidation as evidenced by the doublet peaks of Bi and Te in Figure 7 [69]. Specifically, the O 1s spectrum shown in Figure 7(d) reveals three bonding types at 529.6, 531.7, and 535.8 eV. The higher intensity peak centered at 531.7 eV may be associated with lattice oxygen from metal-oxide bonds in the Bi-Te samples [68, 70–73]. Finally, the minor intensity peaks located at 529.6 and 535.8 eV, correspond to the pair of dangling bonds O^- and O^{2-}, and surface adsorbed oxygen O_2^{2-}, respectively [66, 68–70]. However, it is important to highlight that despite performing the synthesis at atmospheric pressure and a significant low temperature, a high crystallinity has been achieved compared to that reported in other studies [1, 3, 15, 16, 32, 33, 49].

3.6. Thermoelectric Characterization. The measurement of the Seebeck coefficient in thin film depositions like those we have prepared is relatively straightforward. We need to know the temperature difference between two positions on the deposition, and the voltage across these two points [74]. The Seebeck coefficient calculated as function of temperature for a Bi_2Te_3 deposition on FTO substrate is shown in Figure 8. The homemade system used for thermoelectric measurements [35] allows the substrate temperature to vary freely. Every 5 seconds, ΔV and ΔT are measured simultaneously at the instantaneous mean temperature. At the lower limit (300 K), the substrate temperature is practically the same as the reservoir, with a temperature gradient ΔT of ~2 K between the cold and hot ends. At the upper limit (423 K), the substrate temperature is 5 to 7 K higher than the upper limit, and the temperature gradient ΔT between the cold and hot ends is 37 K. Approximately half of this of 37 K difference is within the temperature interval below 423 K (cold side), and the other half above 423 K (hot side). The positive Seebeck coefficient values indicate that the Bi_2Te_3 exhibits a *p*-type conductivity, possibly due to the presence of tellurium secondary phase in the sample, as reported in Section 3.3 [39]. Additionally, an increase in the Seebeck coefficient value is observed within the temperature interval from 300 to 320 K for the deposition, reaching a maximum value of 169.25 μV/K, which is near the room temperature interval. This value is greater in magnitude than those obtained in some reports where Bi_2Te_3 nanoplates were synthesized by a solvothermal process at higher temperatures than the one used in this study [15, 54, 59, 75, 76].

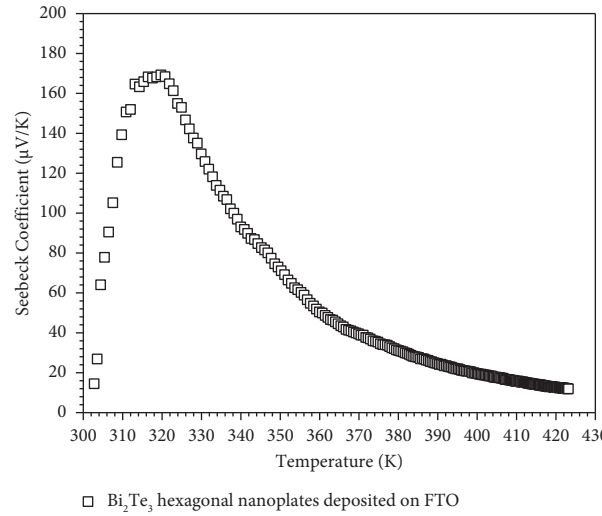

FIGURE 8: Seebeck coefficient calculated as function of temperature.

4. Conclusion

We have prepared Bi_2Te_3 hexagonal nanoplates using a simple convection oven as a reactor, at a lower temperature (140°C) compared to more complex techniques reported by other authors. The crystallographic, structural, chemical, and thermoelectric characteristics of the nanoplates were analyzed. Scanning and transmission electron microscopy verified that bismuth telluride crystallizes in highly crystalline hexagonal nanoplates, with growth along the basal plane of the rhombohedral Bi_2Te_3 structure and a thickness less than the Bohr radius of the bismuth telluride exciton. Raman spectroscopy analysis confirmed this data by exhibiting a peak corresponding to the A_{1u}^2 vibrational mode due to the breaking of the symmetry of the crystal in the direction of the C axis of the $R\bar{3}m$ crystal structure of Bi_2Te_3. X-ray photoelectron spectroscopy results verified the formation of highly crystalline Bi_2Te_3, despite the strong reactivity of the Te^{2-} ion precursor with ambient oxygen. Finally, X-ray diffraction analysis confirmed the crystalline phase of Bi_2Te_3 nanoplates, as reported in the electron microscopy and Raman spectroscopy sections. and indicated the presence of a tellurium secondary phase in the Bi_2Te_3 deposition. This secondary phase influenced the *p*-type conductivity observed in the sample. Thermoelectric characterization of the Bi_2Te_3/FTO deposition yielded a maximum Seebeck coefficient of 169 μV/K, a value achieved near room temperature and greater in magnitude than other reports based on solvothermal synthesis of Bi_2Te_3 hexagonal nanoplates.

Data Availability

All data generated or analyzed during this study are included in this published manuscript.

Ethical Approval

This research contains no animal or human studies conducted by any of the authors.

Conflicts of Interest

The authors declare that they have no conflicts of interest.

Authors' Contributions

All authors contributed equally to this work.

Acknowledgments

The authors would like to thank Norberto Hernandez Como and Raul Borja-Urby from the Center of Nanosciences and Micro- and Nanotechnologies, Polytechnic Institute of Mexico (CNMN-IPN), for their technical support in TEM and SEM measurements; Eduardo Martinez Guerra and Lilia Magdalena Bautista-Carrillo (CIMAV-Monterrey) for their assistance; Jose Antonio Rivera Mayorga (University of Guadalajara) for his support in XPS analysis; and Cecilia Sanchez and Jose Santos Cruz for their support on IR and Raman spectroscopy measurements. This research was funded by the National Council for Science and Technology (CONAHCYT-Mexico) through postdoctoral grants (BP-PA-20220902131114325-3642215) and (BP-PA-20220705150715748-2482439). Additional support for XPS analysis was provided by CONAHCYT grant (270662).

References

[1] Y. Liu, Y. Zhang, K. H. Lim et al., "High thermoelectric performance in crystallographically textured n-type $Bi_2Te_{3-x}Se_x$ produced from asymmetric colloidal nanocrystals," *ACS Nano*, vol. 12, no. 7, pp. 7174–7184, 2018.

[2] P. Seferlis, P. S. Varbanov, A. I. Papadopoulos, H. H. Chin, and J. J. Klemeš, "Sustainable design, integration, and operation for energy high-performance process systems," *Energy*, vol. 224, Article ID 120158, 2021.

[3] C. Hollar, Z. Lin, M. Kongara et al., "High-performance flexible bismuth telluride thin film from solution processed, colloidal nanoplates," *Advanced Materials Technologies*, vol. 5, no. 11, Article ID 2000600, 2020.

[4] D. Zhao, A. Würger, and X. Crispin, "Ionic thermoelectric materials and devices," *Journal of Energy Chemistry*, vol. 61, pp. 88–103, 2021.

[5] S. Madruga, "Enhancement of thermoelectric energy harvesting of thermal fluctuations with thermocapillary flows in phase-change materials embedded in metallic foams," *European Physical Journal: Special Topics*, vol. 232, no. 4, pp. 395–402, 2023.

[6] S. Kim, S. Yamamoto, and T. Aizawa, "Thermoelectric properties of anisotropy-controlled p-type Bi–Te–Sb system via bulk mechanical alloying and shear extrusion," *Journal of Alloys and Compounds*, vol. 375, no. 1-2, pp. 107–113, 2004.

[7] B. Dzundza, L. Nykyruy, T. Parashchuk et al., "Transport and thermoelectric performance of n-type PbTe films," *Physica B: Condensed Matter*, vol. 588, Article ID 412178, 2020.

[8] S. Ortega, M. Ibáñez, Y. Liu et al., "Bottom-up engineering of thermoelectric nanomaterials and devices from solution-processed nanoparticle building blocks," *Chemical Society Reviews*, vol. 46, no. 12, pp. 3510–3528, 2017.

[9] L. Yang, Z.-G. Chen, M. S. Dargusch, and J. Zou, "High performance thermoelectric materials: Progress and their applications," *Advanced Energy Materials*, vol. 8, no. 6, 2017.

[10] D. Ding, C. Lu, and Z. Tang, "Bottom-up chalcogenide thermoelectric materials from solution-processed nanostructures," *Advanced Materials Interfaces*, vol. 4, no. 20, 2017.

[11] M. J. Carter, A. El-Desouky, M. A. Andre, P. Bardet, and S. LeBlanc, "Pulsed laser melting of bismuth telluride thermoelectric materials," *Journal of Manufacturing Processes*, vol. 43, pp. 35–46, 2019.

[12] M. Takashiri, M. Takiishi, S. Tanaka, K. Miyazaki, and H. Tsukamoto, "Thermoelectric properties of n-type nanocrystalline bismuth-telluride-based thin films deposited by flash evaporation," *Journal of Applied Physics*, vol. 101, no. 7, 2007.

[13] J. X. Zhang, Q. Li, P. J. Niu et al., "Effect of annealing temperature on microstructure and thermoelectric properties of bismuth–telluride multilayer thin films prepared by magnetron sputtering," *Materials Research Innovations*, vol. 19, no. sup10, pp. S10-S408–S10-412, 2015.

[14] K. Kusagaya, H. Hagino, S. Tanaka, K. Miyazaki, and M. Takashiri, "Structural and thermoelectric properties of nanocrystalline bismuth telluride thin films under compressive and tensile strain," *Journal of Electronic Materials*, vol. 44, no. 6, pp. 1632–1636, 2014.

[15] K. Wada, K. Tomita, and M. Takashiri, "Fabrication of bismuth telluride nanoplates via solvothermal synthesis using different alkalis and nanoplate thin films by printing method," *Journal of Crystal Growth*, vol. 468, pp. 194–198, 2017.

[16] M. Takashiri, S. Kai, K. Wada, S. Takasugi, and K. Tomita, "Role of stirring assist during solvothermal synthesis for preparing single-crystal bismuth telluride hexagonal nanoplates," *Materials Chemistry and Physics*, vol. 173, pp. 213–218, 2016.

[17] H. Kaur, L. Sharma, S. Singh, B. Sivaiah, G. B. Reddy, and T. D. Senguttuvan, "Enhancement in figure of merit (ZT) by annealing of BiTe nanostructures synthesized by microwave-assisted flash combustion," *Journal of Electronic Materials*, vol. 43, no. 6, pp. 1782–1789, 2013.

[18] S. Pradhan, R. Das, R. Bhar, R. Bandyopadhyay, and P. Pramanik, "A simple fast microwave-assisted synthesis of thermoelectric bismuth telluride nanoparticles from homogeneous reaction-mixture," *Journal of Nanoparticle Research*, vol. 19, no. 2, p. 69, 2017.

[19] B. Hamawandi, H. Mansouri, S. Ballikaya et al., "A comparative study on the thermoelectric properties of bismuth chalcogenide alloys synthesized through mechanochemical alloying and microwave-assisted solution synthesis routes," *Frontiers in Materials*, vol. 7, 2020.

[20] B. Hamawandi, H. Batili, M. Paul et al., "Minute-made, high-efficiency nanostructured Bi_2Te_3 via high-throughput green solution chemical synthesis," *Nanomaterials*, vol. 11, no. 8, p. 2053, 2021.

[21] A. Sharma, A. K. Srivastava, T. D. Senguttuvan, and S. Husale, "Robust broad spectral photodetection (UV-NIR) and ultra high responsivity investigated in nanosheets and nanowires of Bi_2Te_3 under harsh nano-milling conditions," *Scientific Reports*, vol. 7, no. 1, Article ID 17911, 2017.

[22] J. Yao, J. Shao, Y. Wang, Z. Zhao, and G. Yang, "Ultra-broadband and high response of the Bi_2Te_3-Si heterojunction and its application as a photodetector at room temperature in

harsh working environments," *Nanoscale*, vol. 7, no. 29, pp. 12535–12541, 2015.

[23] Y. L. Chen, J. G. Analytis, J.-H. Chu et al., "Experimental realization of a three-dimensional topological insulator, Bi_2Te_3," *Science*, vol. 325, no. 5937, pp. 178–181, 2009.

[24] J. M. Raju and K. J. Thomas, "Topological insulator phases in polycrystalline Bi_2Te_3 thin films," *AIP Advances*, vol. 13, no. 2, 2023.

[25] A. I. Figueroa, G. Van der Laan, S. E. Harrison, G. Cibin, and T. Hesjedal, "Oxidation effects in rare earth doped topological insulator thin films," *Scientific Reports*, vol. 6, no. 1, Article ID 22935, 2016.

[26] M. R. Amin Bhuiyan, H. Mamur, and Ö. F. Dilmaç, "DA review on performance evaluation of Bi_2Te_3-based and some other thermoelectric nanostructured materials," *Current Nanoscience*, vol. 17, no. 3, pp. 423–446, 2021.

[27] S. Yonezawa, T. Tabuchi, and M. Takashiri, "Atomic composition changes in bismuth telluride thin films by thermal annealing and estimation of their thermoelectric properties using experimental analyses and first-principles calculations," *Journal of Alloys and Compounds*, vol. 841, Article ID 155697, 2020.

[28] J. S. Son, M. K. Choi, M.-K. Han et al., "n-Type nanostructured thermoelectric materials prepared from chemically synthesized ultrathin Bi_2Te_3 nanoplates," *Nano Letters*, vol. 12, no. 2, pp. 640–647, 2012.

[29] M. Hong, Z.-G. Chen, L. Yang, and J. Zou, "Enhancing thermoelectric performance of Bi_2Te_3-based nanostructures through rational structure design," *Nanoscale*, vol. 8, no. 16, pp. 8681–8686, 2016.

[30] T. Wang, R. Mehta, C. Karthik et al., "Microsphere bouquets of bismuth telluride nanoplates: Room-temperature synthesis and thermoelectric properties," *Journal of Physical Chemistry C*, vol. 114, no. 4, pp. 1796–1799, 2010.

[31] Z. Sun, S. Liufu, Q. Yao, and L. Chen, "Low temperature synthesis of Bi_2Te_3 nanosheets and thermal conductivity of nanosheet-contained composites," *Materials Chemistry and Physics*, vol. 121, no. 1-2, pp. 138–141, 2010.

[32] P. Srivastava and K. Singh, "Low temperature reduction route to synthesise bismuth telluride (Bi2Te3) nanoparticles: Structural and optical studies," *Journal of Experimental Nanoscience*, vol. 9, no. 10, pp. 1064–1074, 2014.

[33] X. He, H. Zhang, W. Lin et al., "PVP-assisted solvothermal synthesis of high-yielded Bi_2Te_3 hexagonal nanoplates: Application in passively Q-switched fiber laser," *Scientific Reports*, vol. 5, no. 1, Article ID 15868, 2015.

[34] Y. Zhang, Q. You, W. Huang et al., "Few-layer hexagonal bismuth telluride (Bi_2Te_3) nanoplates with high-performance UV-Vis photodetection," *Nanoscale Advances*, vol. 2, no. 3, pp. 1333–1339, 2020.

[35] E. Díaz-Torres, A. Flores-Conde, A. Ávila-García, and M. Ortega-López, "Electronic transport study of PbSe pellets prepared from self-assembled 2D-PbSe nanostructures," *Current Applied Physics*, vol. 18, no. 2, pp. 226–230, 2018.

[36] I. Bejenari, V. Kantser, and A. A. Balandin, "Thermoelectric properties of electrically gated bismuth telluride nanowires," *Physical Review B: Condensed Matter*, vol. 81, no. 7, Article ID 075316, 2010.

[37] Y. Deng, C.-W. Nan, G.-D. Wei, L. Guo, and Y. Lin, "Organic-assisted growth of bismuth telluride nanocrystals," *Chemical Physics Letters*, vol. 374, no. 3-4, pp. 410–415, 2003.

[38] H. Zhang, C. Liu, X. Qi, X. Dai, Z. Fang, and S. Zhang, "Topological insulators in Bi_2Se_3, Bi_2Te_3 and Sb_2Te_3 with a single Dirac cone on the surface," *Nature Physics*, vol. 5, no. 6, pp. 438–442, 2009.

[39] V. Thakur, K. Upadhyay, R. Kaur, N. Goyal, and S. Gautam, "Investigating phase transition and morphology of Bi-Te thermoelectric system," *Materials Today Advances*, vol. 8, Article ID 100082, 2020.

[40] W. Richter and C. R. Becker, "A Raman and far-infrared investigation of phonons in the rhombohedral V_2–VI_3 compounds Bi_2Te_3, Bi_2Se_3, Sb_2Te_3 and $Bi_2(Te_{1-x}Se_x)_3$ $(0 < x < 1)$, $(Bi_{1-y}Sb_y)_2Te_3$ $(0 < y < 1)$," *Physica Status Solidi (B)*, vol. 84, no. 2, pp. 619–628, 1977.

[41] W. Kullmann, J. Geurts, W. Richter et al., "Effect of hydrostatic and uniaxial pressure on structural properties and Raman active lattice vibrations in Bi_2Te_3," *Physica Status Solidi (B)*, vol. 125, no. 1, pp. 131–138, 1984.

[42] V. Russo, A. Bailini, M. Zamboni et al., "Raman spectroscopy of Bi-Te thin films," *Journal of Raman Spectroscopy*, vol. 39, no. 2, pp. 205–210, 2008.

[43] L. M. Goncalves, C. Couto, P. Alpuim, A. G. Rolo, F. Völklein, and J. H. Correia, "Optimization of thermoelectric properties on Bi_2Te_3 thin films deposited by thermal co-evaporation," *Thin Solid Films*, vol. 518, no. 10, pp. 2816–2821, 2010.

[44] K. M. F. Shahil, M. Z. Hossain, D. Teweldebrhan, and A. A. Balandin, "Crystal symmetry breaking in few-quintuple Bi_2Te_3 films: Applications in nanometrology of topological insulators," *Applied Physics Letters*, vol. 96, no. 15, 2010.

[45] L. Ren, X. Qi, Y. Liu et al., "Large-scale production of ultrathin topological insulator bismuth telluride nanosheets by a hydrothermal intercalation and exfoliation route," *Journal of Materials Chemistry*, vol. 22, no. 11, pp. 4921–4926, 2012.

[46] X. Luo, M. B. Sullivan, and S. Y. Quek, "First-principles investigations of the atomic, electronic, and thermoelectric properties of equilibrium and strained Bi_2Se_3 and Bi_2Te_3 including van der Waals interactions," *Physical Review B: Condensed Matter*, vol. 86, no. 18, Article ID 184111, 2012.

[47] V. Wagner, G. Dolling, B. M. Powell, and G. Landweher, "Lattice vibrations of Bi_2Te_3," *Physica Status Solidi (B)*, vol. 85, no. 1, pp. 311–317, 1978.

[48] P. Y. Yu and M. Cardona, *Fundamentals of Semiconductors-Physics and Materials Properties*, Springer, Heidelberg, Germany, 3rd edition, 2005.

[49] M. R. A. Bhuiyan and H. Mamur, "Bismuth telluride (Bi_2Te_3) nanostructure for thermoelectric applications," *International Scientific and Vocational Studies Journal*, vol. 3, pp. 1–7, 2019.

[50] Y. Liang, W. Wang, B. Zeng et al., "Raman scattering investigation of Bi_2Te_3 hexagonal nanoplates prepared by a solvothermal process in the absence of NaOH," *Journal of Alloys and Compounds*, vol. 509, no. 16, pp. 5147–5151, 2011.

[51] S. Anwar, B. K. Mishra, and S. Anwar, "Thermoelectric performance of Bi_2Te_3, Sb_2Te_3 thin film," *Advanced Materials Proceedings*, vol. 1, pp. 191–194, 2016.

[52] C. D. Gutiérrez-Lazos, F. Solís-Pomar, M. F. Meléndrez et al., "A simple method for the deposition of nanostructured tellurium synthesized in ammonia solution," *Applied Nanoscience*, vol. 6, no. 7, pp. 1053–1057, 2016.

[53] P. T. C. Freire, M. A. Araújo Silva, V. C. S. Reynoso, A. R. Vaz, and V. Lemos, "Pressure Raman scattering of CdTe quantum dots," *Physical Review B: Condensed Matter*, vol. 55, no. 11, pp. 6743–6746, 1997.

[54] A. Subrati, Y. Kim, Y. F. AlWahedi et al., "Monitoring the multiphasic evolution of bismuth telluride nanoplatelets," *CrystEngComm*, vol. 22, no. 45, pp. 7918–7928, 2020.

[55] W. Lu, Y. Ding, Y. Chen, Z. L. Wang, and J. Fang, "Bismuth telluride hexagonal nanoplatelets and their two-step epitaxial

growth," *Journal of the American Chemical Society*, vol. 127, no. 28, pp. 10112–10116, 2005.

[56] E. Ashalley, H. Chen, X. Tong, H. Li, and Z. M. Wang, "Bismuth telluride nanostructures: Preparation, thermoelectric properties and topological insulating effect," *Frontiers of Materials Science*, vol. 9, no. 2, pp. 103–125, 2015.

[57] Y. Saberi, S. A. Sajjadi, and H. Mansouri, "Comparison of characteristics of Bi_2Te_3 and $Bi_2Te_{2.7}Se_{0.3}$ thermoelectric materials synthesized by hydrothermal process," *Journal of Materials Science: Materials in Electronics*, vol. 31, no. 21, pp. 18988–18995, 2020.

[58] J. Yang, T. Xie, C. Liu, and L. Xu, "Facile fabrication of dumbbell-like β-Bi_2O_3/graphene nanocomposites and their highly efficient photocatalytic activity," *Materials*, vol. 11, no. 8, p. 1359, 2018.

[59] J. Fu, S. Song, X. Zhang et al., "Bi_2Te_3 nanoplates and nanoflowers: synthesized by hydrothermal process and their enhanced thermoelectric properties," *CrystEngComm*, vol. 14, no. 6, pp. 2159–2165, 2012.

[60] D. Park, H. Ju, Y. Kim, and J. Kim, "A strategy for low thermal conductivity and enhanced thermoelectric power factor in one-dimensional Bi_2Te_3/Cu_2Te nanowire composites," *Journal of Materials Science: Materials in Electronics*, vol. 30, no. 14, pp. 13297–13304, 2019.

[61] B. Trawiński, B. Bochentyn, M. Łapiński, and B. Kusz, "A study of the kinetics of bismuth telluride synthesis by an oxide reduction method," *Thermochimica Acta*, vol. 683, Article ID 178437, 2020.

[62] P. Ngabonziza, R. Heimbuch, N. de Jong et al., "In situ spectroscopy of intrinsic Bi_2Te_3 topological insulator thin films and impact of extrinsic defects," *Physical Review B: Condensed Matter*, vol. 92, no. 3, Article ID 035405, 2015.

[63] H. Bando, K. Koizumi, Y. Oikawa, K. Daikohara, V. A. Kulbachinskii, and H. Ozaki, "The time-dependent process of oxidation of the surface of Bi_2Te_3 studied by x-ray photoelectron spectroscopy," *Journal of Physics: Condensed Matter*, vol. 12, no. 26, pp. 5607–5616, 2000.

[64] M. K. Bahl, R. L. Watson, and K. J. Irgolic, "X-ray photoemission studies of tellurium and some of its compounds," *The Journal of Chemical Physics*, vol. 66, no. 12, pp. 5526–5535, 1977.

[65] M. Ahmad, K. Agarwal, and B. R. Mehta, "An anomalously high Seebeck coefficient and power factor in ultrathin Bi_2Te_3 film: Spin–orbit interaction," *Journal of Applied Physics*, vol. 128, no. 3, Article ID 035108, 2020.

[66] E. A. Hoffmann, T. Körtvélyesi, E. Wilusz, L. S. Korugic-Karasz, F. E. Karasz, and Z. A. Fekete, "Relation between C1s XPS binding energy and calculated partial charge of carbon atoms in polymers," *Journal of Molecular Structure: THEOCHEM*, vol. 725, no. 1-3, pp. 5–8, 2005.

[67] Y.-G. Lei, K.-M. Ng, L.-T. Weng, C.-M. Chan, and L. Li, "XPS C 1s binding energies for fluorocarbon-hydrocarbon microblock copolymers," *Surface and Interface Analysis*, vol. 35, no. 10, pp. 852–855, 2003.

[68] G. Beamson and D. Briggs, *High Resolution XPS of Organic Polymers: The Scienta ESCA300 Database*, Wiley, New York, NY, USA, 1992.

[69] R. Zheng, W. Cheng, E. Wang, and S. Dong, "Synthesis of tellurium nanorods via spontaneous oxidation of NaHTe at room temperature," *Chemical Physics Letters*, vol. 395, no. 4-6, pp. 302–305, 2004.

[70] G. P. López, D. G. Castner, and B. D. Ratner, "XPS O 1s binding energies for polymers containing hydroxyl, ether, ketone and ester groups," *Surface and Interface Analysis*, vol. 17, no. 5, pp. 267–272, 1991.

[71] R. A. H. El-Mallawany, *Tellurite Glasses Handbook: Physical Properties and Data*, CRC Press, Boca Raton, FL, USA, 2nd edition, 2018.

[72] B. R. MacDougall, R. S. Alwitt, and T. A. Ramanarayanan, *Proceedings of the Symposium on Oxide Films on Metals and Alloys (Proceedings/Electrochemical Society)*, Electrochemical Society, Pennington, NJ, USA, 1992.

[73] J. Kim, L. T. Duy, B. Ahn, and H. Seo, "Pre-oxidation effects on properties of bismuth telluride thermoelectric composites compacted by spark plasma sintering," *Journal of Asian Ceramic Societies*, vol. 8, no. 1, pp. 211–221, 2020.

[74] S. Iwanaga, E. S. Toberer, A. LaLonde, and G. Snyder, "A high temperature apparatus for measurement of the Seebeck coefficient," *Review of Scientific Instruments*, vol. 82, no. 6, Article ID 063905, 2011.

[75] L. Yang, Z.-G. Chen, M. Hong, G. Han, and J. Zou, "Enhanced thermoelectric performance of nanostructured Bi_2Te_3 through significant phonon scattering," *ACS Applied Materials and Interfaces*, vol. 7, no. 42, pp. 23694–23699, 2015.

[76] R. Mori, Y. Mayuzumi, M. Yamaguchi, A. Kobayashi, Y. Seki, and M. Takashiri, "Improved thermoelectric properties of solvothermally synthesized Bi_2Te_3 nanoplate films with homogeneous interconnections using Bi_2Te_3 electrodeposited layers," *Journal of Alloys and Compounds*, vol. 818, Article ID 152901, 2020.